Chiral NNLO_{sat} descriptions of nuclear multipole resonances within the random-phase approximation

Q. Wu, B. S. Hu, F. R. Xu, Y. Z. Ma, S. J. Dai, Z. H. Sun, and G. R. Jansen

Phys. Rev. C **97**, 054306 — Published 3 May 2018

DOI: 10.1103/PhysRevC.97.054306

Chiral $\mathrm{NNLO_{sat}}$ descriptions of nuclear multipole resonances within the random phase approximation

Q. Wu,[1] B. S. Hu,[1] F. R. Xu,[1,*] Y. Z. Ma,[1] S. J. Dai,[1] Z.H. Sun,[1,2,3] and G. R. Jansen[4,3,†]

[1]*School of Physics, and State Key Laboratory of Nuclear Physics and Technology, Peking University, Beijing 100871, China*

[2]*Department of Physics and Astronomy, University of Tennessee, Knoxville, Tennessee 37996, USA*

[3]*Physics Division, Oak Ridge National Laboratory, Oak Ridge, Tennessee 37831, USA*

[4]*National Center for Computational Sciences, Oak Ridge National Laboratory, Oak Ridge, TN 37831, USA*

(Dated: April 18, 2018)

Abstract

We study nuclear multipole resonances in the framework of the random phase approximation using the chiral potential $\mathrm{NNLO_{sat}}$. This potential includes two- and three-body terms that has been simultaneously optimized to low-energy nucleon-nucleon scattering data and selected nuclear structure data. Our main foci have been the isoscalar monopole, isovector dipole, and isoscalar quadrupole resonances of the closed-shell nuclei, ^{4}He, ^{16,22,24}O, and ^{40,48}Ca. These resonance modes have been widely observed in experiment. In addition, we use a renormalized chiral potential $V_{\text{low-}k}$, based on the N^{3}LO two-body potential by Entem and Machleidt [Phys. Rev. **C68**, 041001 (2011)]. This introduces a dependency on the cutoff parameter used in the normalization procedure as reported in previous works by other groups. While $\mathrm{NNLO_{sat}}$ can reasonably reproduce observed multipole resonances, it is not possible to find a single cutoff parameter for the $V_{\text{low-}k}$ potential that simultaneously describe the different types of resonance modes. The sensitivity to the cutoff parameter can be explained by missing induced three-body forces in the calculations. Our results for neutron-rich ^{22,24}O show a mixing nature of isoscalar and isovector resonances in the dipole channel at low energies. We predict that ^{22}O and ^{24}O have low-energy isoscalar quadrupole resonances at energies lower than 5 MeV.

* frxu@pku.edu.cn

I. INTRODUCTION

The occurrence of collective resonances is a common phenomenon of many-body quantum systems. At excitation energies above particle thresholds, the response of the nucleus to an external nuclear or electromagnetic field is dominated by collective vibrations of various multipolarities. The isovector giant dipole resonance (IVGDR) [1–3] was one of the earliest collective vibrational modes observed in nuclei. In IVGDR, the protons and neutrons oscillate against each other in a dipole mode [4]. Giant resonances can occur on the whole nuclear chart and are directly connected to bulk properties of nuclei, such as incompressibility and symmetry energy [5–8]. For neutron-rich isotopes, there exist electric dipole ($E1$) responses at low energy with weak strengths, named pigmy dipole resonances (PDR) [9]. These are interpreted as dipole oscillations of excess neutrons against the $N = Z$ proton-neutron saturated core [10]. Furthermore, in weakly-bound nuclei along the driplines, it has been speculated that there exist resonances called soft dipole resonances [11], a dipole mode where loosely-bound nucleons oscillate against a core. The soft resonances can occur at even lower energies, attracting much interest in both theory [12–14] and experiments [15–17]. A soft dipole resonance has been observed in the halo nucleus ^{11}Li at an excitation energy of only 1.03 MeV [16]. Low-energy monopole and quadrupole resonances have also been observed in neutron-rich nuclei (see e.g. Refs. [18–20]). A microscopic description of multipole resonances, based on realistic nuclear forces, is challenging because of the computational complexity involved in solving the nuclear many-body problem.

Within the Hartree-Fock (HF) approach with non-relativistic Skyrme or relativistic meson-exchange potential, the random phase approximation (RPA) which describes nuclear collective vibrations by particle-hole excitations, has been successfully applied to describe multipole responses in nuclei (see e.g. the reviews [14, 21, 22] and references therein). However, details of the calculations depend on nuclear forces used. Especially, the calculations of low-lying resonance strengths can be drastically different with different forces. For example, it was pointed out that the tensor force in the Skyrme interaction has a significant effect on charge-exchange dipole excitations [23], while the tensor force is missing in many other calculations. In theory, the collective responses of nuclei are directly related to certain properties of the underlying nuclear force.

Recent nuclear structure calculations have highlighted the use of realistic nuclear forces

that accurately describe nucleon-nucleon scattering. The giant dipole resonances (GDR) of ^{3}H, ^{3}He, and ^{4}He, have been investigated within the framework of the correlated hyperspherical harmonic expansion [24, 25], using the Argonne AV18 [26] two-body (NN) potential plus the Urbana [27] three-body (NNN) force. It was found that three-body forces had a strong effect in the region of excitation energies higher than 50 MeV. The ^{4}He giant resonances were further studied by the no core shell model [28] and with the effective interaction hyperspherical harmonics method [29], using interactions from chiral effective field theory (EFT). In heavier nuclei, the random phase approximation based on realistic forces has been successful. In Refs. [30–33], a correlated interaction derived from the AV18 potential by using the unitary correlation operator method (UCOM) [34] was used with HF-RPA. These calculations reproduced experimental multipole resonances reasonably well, but the details depended on the UCOM cutoff parameter of the potential.

The dipole resonances of closed-shell nuclei have also been studied using the coupled-cluster approach with chiral forces [35, 36]. Chiral effective field theory offers a consistent framework to derive two- and three-nucleon forces. Recently, the Oak Ridge group suggested a chiral EFT potential called NNLO$_{\rm sat}$ where two-nucleon and three-nucleon forces were optimized simultaneously to low-energy nucleon-nucleon scattering data, as well as binding energies and radii of few-nucleon systems and selected isotopes of carbon and oxygen [37]. This potential has been successfully used to describe the electric dipole polarizabilities of ^{4}He, ^{40}Ca and ^{16,22}O [38, 39].

The RPA has been proved to be an efficient approximation to describe collective resonances and long-range correlations. The low computational cost makes it feasible to describe multipole resonances of medium-mass nuclei. These resonances are considered using a one-body operator response of the nucleus, thus the resonance strength should come mainly from one-particle one-hole ($1p1h$) excitations. In this paper, we perform self-consistent HF-RPA calculations with the chiral NNLO$_{\rm sat}$ potential and describe multipole resonances of closed-shell helium, oxygen and calcium isotopes. In this context, self-consistence means that the HF and RPA calculations are performed using the same interaction. However, the three-nucleon force has only been included fully in the Hartree-Fock calculations, while in the RPA calculations we keep only the normal-ordered zero-, one-, and two-body terms of the three-body force [40, 41]. For comparison, we also performed HF-RPA calculations with a chiral two-body N^{3}LO potential [42, 43] renormalized by the $V_{\text{low-}k}$ technique [44] at

different low-momentum cutoff parameters.

II. THEORETICAL FRAMEWORK

A. The RPA formulation

The RPA equations can be derived within different theoretical frameworks such as Green's function theory, the small amplitude limit of time-dependent Hartree Fock (TDHF) and equation of motion (EOM). In the framework of EOM, the details of the RPA formulation can be found in a standard textbook [45]. In this paper, we briefly state the RPA equations in an angular momentum coupled representation. The A-body intrinsic Hamiltonian can be written as

$$\begin{aligned} H &= \sum_{i=1}^{A} \frac{\boldsymbol{p}_i^2}{2m} + \sum_{i<j=1}^{A} V_{ij} - \frac{(\sum_{i=1}^{A} \boldsymbol{p}_i)^2}{2mA} + \sum_{i<j<k=1}^{A} W_{ijk} \\ &= (1-\frac{1}{A}) \sum_{i=1}^{A} \frac{\boldsymbol{p}_i^2}{2m} + \sum_{i<j=1}^{A} (V_{ij} - \frac{\boldsymbol{p}_i \cdot \boldsymbol{p}_j}{mA}) + \sum_{i<j<k=1}^{A} W_{ijk}, \end{aligned} \tag{1}$$

where m is the average mass of a nucleon, A is the mass number of the nucleus, $\boldsymbol{p}_i$ is the nucleon momentum in the laboratory frame, V_{ij} is the two-body nucleon-nucleon force, and W_{ijk} is the three-nucleon force.

We first perform a spherical HF calculation for the full Hamiltonian (1) in the harmonic oscillator (HO) basis. In spherical case, the angular momentum is preserved. In the HF numerical iteration, the three-nucleon force and center-of-mass correction remain included, i.e., we are performing the HF calculation with three-nucleon force and center-of-mass correction. After the HF calculation, the three-nucleon force is written in a normal-ordered form in the HF basis as [40, 41]

$$\begin{aligned} W_{\rm NO} =& \frac{1}{6} \sum_{ijk} \langle ijk|W|ijk\rangle + \frac{1}{2} \sum_{ijps} \langle pij|W|sij\rangle \{a_p^\dagger a_s\} + \frac{1}{4} \sum_{ipqst} \langle pqi|W|sti\rangle \{a_p^\dagger a_q^\dagger a_t a_s\} + \\ & \frac{1}{36} \sum_{pqrstu} \langle pqr|W|stu\rangle \{a_p^\dagger a_q^\dagger a_r^\dagger a_u a_t a_s\}, \end{aligned} \tag{2}$$

where $\hat{a}_q^\dagger$ and $\hat{a}_q$ are operators that respectively create and annihilate a particle in the HF single-particle state labelled by q, and the symbol $\{\ldots\}$ indicates the normal-ordered form of the operators with respect to the HF ground state. We can see that in the normal-ordered

form the three-nucleon force separates into a zero-, one-, two- and three-body terms. In the present RPA calculations, we consider the effects of the three-nucleon force at the normal-ordered two-body level [40, 41], while the residual three-body term (i.e., the last term in Eq. (2)) is neglected. Then we obtain a two-body Hamiltonian but including normal-ordered three-nucleon forces and center-of-mass correction, for the RPA calculation,

$$H = E_{\rm HF} + \sum_s \epsilon_s \{\hat{a}_s^\dagger \hat{a}_s\} + \frac{1}{4}\sum_{pqst} \langle pq|V|st\rangle \{\hat{a}_p^\dagger \hat{a}_q^\dagger \hat{a}_t \hat{a}_s\}, \tag{3}$$

where $E_{\rm HF}$ is the HF ground-state energy, and V is the nucleon-nucleon interaction with contributions from the normal-ordered three-nucleon force, and ϵ_s are the HF single-particle energies. Effects from the three-nucleon force and center-of-mass correction appear in all the terms, i.e., $E_{\rm HF}$, ϵ_s and $\langle pq|V|st\rangle$ in the Hamiltonian (3). The excited states can be written as

$$|\nu, JM\rangle = Q^\dagger_{\nu,JM}|0\rangle, \tag{4}$$

where $|0\rangle$ is the ground state. The operator $Q^\dagger_{\nu,JM}$ creates excited states with angular momentum J and its projection M and other quantum numbers (ν). In the RPA, this operator is approximated as

$$Q^\dagger_{\nu,JM} = \sum_{ph} \left[X^{\nu,JM}_{ph} A^{JM\dagger}_{ph} - (-1)^{J+M} Y^{\nu,JM}_{ph} A^{J,-M}_{ph} \right], \tag{5}$$

where $X^{\nu,JM}_{ph}$ and $Y^{\nu,JM}_{ph}$ are forward and backward-going particle-hole amplitudes of the state (ν, JM), respectively. The labels ph represents $1p1h$ excitations, and the operator $A^{JM\dagger}_{ph}$ couples the $1p1h$ configuration to the angular momentum J and projection M. The summation runs over all allowed $1p1h$ excitations with (JM) in the model space. The operator $A^{JM\dagger}_{ph}$ can be expressed in the HF basis as

$$A^{JM\dagger}_{ph} = \sum_{m_p m_h} (-1)^{j_h - m_h} \langle j_p m_p, j_h \ -m_h | JM\rangle \hat{a}^\dagger_{j_p m_p} \hat{a}_{j_h m_h}, \tag{6}$$

where j and m are the total angular momentum and its projection of a HF single-particle state, with p for a particle state and h for a hole state.

The EOM [46] gives a set of coupled equations for the amplitude vectors $\boldsymbol{X}^{\nu,J}$ and $\boldsymbol{Y}^{\nu,J}$,

$$\begin{pmatrix} \mathbf{A}^J & \mathbf{B}^J \\ -\mathbf{B}^{J*} & -\mathbf{A}^{J*} \end{pmatrix} \begin{pmatrix} \boldsymbol{X}^{\nu,J} \\ \boldsymbol{Y}^{\nu,J} \end{pmatrix} = \hbar\Omega_\nu \begin{pmatrix} \mathbf{G}^J & \mathbf{0} \\ \mathbf{0} & \mathbf{G}^{J*} \end{pmatrix} \begin{pmatrix} \boldsymbol{X}^{\nu,J} \\ \boldsymbol{Y}^{\nu,J} \end{pmatrix}, \tag{7}$$

where $\hbar\Omega_\nu$ is the excitation energy of the ν-th eigen state $(\boldsymbol{X}^{\nu,J}, \boldsymbol{Y}^{\nu,J})$. The matrices are given by their matrix elements

$$\begin{aligned}
\mathbf{A}^J_{ph,p'h'} &= \langle 0|[A^{JM}_{ph}, H, A^{JM\dagger}_{p'h'}]|0\rangle, \\
\mathbf{B}^J_{ph,p'h'} &= -\langle 0|[A^{JM}_{ph}, H, (-1)^{J+M} A^{J,-M}_{p'h'}]|0\rangle, \\
\mathbf{G}^J_{ph,p'h'} &= \langle 0|[A^{JM}_{ph}, A^{JM\dagger}_{p'h'}]|0\rangle,
\end{aligned} \tag{8}$$

where the double commutator $[A, B, C]$ is defined as $2[A, B, C] = [A, [B, C]] + [[A, B], C]$ [46], and $|0\rangle$ is the correlated ground state.

The ground state in Eq. (8) can be approximated in different ways. If we approximate it by the HF ground state $|0\rangle = |\mathrm{HF}\rangle$, it is usually known as the quasi-boson (QB) approximation, and we obtain the matrix elements as done in the standard RPA,

$$\begin{aligned}
\mathbf{A}^J_{ph,p'h'} &= (\epsilon_p - \epsilon_h)\delta_{pp'}\delta_{hh'} + \langle ph^{-1}, J|V|p'h'^{-1}, J\rangle, \\
\mathbf{B}^J_{ph,p'h'} &= \langle ph^{-1}, J|V|p'^{-1}h', J\rangle, \\
\mathbf{G}^J_{ph,p'h'} &= \delta_{pp'}\delta_{hh'},
\end{aligned} \tag{9}$$

where ϵ_p and ϵ_h are the energies of the HF single-particle and -hole states, respectively. The cross-coupled matrix elements are defined as follows,

$$\begin{aligned}
\langle ac^{-1}, J|V|b^{-1}d, J\rangle &\equiv (-1)^{j_b - j_d + J}\langle ac^{-1}, J|V|db^{-1}, J\rangle \\
&\equiv \sum_{J'}(2J'+1)(-1)^{j_b + j_c + J + J'} \begin{Bmatrix} j_a & j_c & J \\ j_d & j_b & J' \end{Bmatrix}_{6j} \times \\
&\qquad \sqrt{(1+\delta_{ab})(1+\delta_{cd})}\langle ab, J'|V|cd, J'\rangle,
\end{aligned} \tag{10}$$

where a, b, c and d indicate the HF single-particle states, and $\langle ab, J'|V|cd, J'\rangle$ is the coupled nucleon-nucleon interaction matrix element defined by

$$\begin{aligned}
\langle ab, J'|V|cd, J'\rangle = \sum_{m_a m_b m_c m_d} &\langle j_a m_a, j_b m_b|J'M\rangle\langle j_c m_c, j_d m_d|J'M\rangle \times \\
&\frac{1}{\sqrt{(1+\delta_{ab})(1+\delta_{cd})}}\langle ab|V|cd\rangle
\end{aligned} \tag{11}$$

In the QB approximation, the double commutators are calculated using the HF ground state rather than the actual yet unknown ground state, which is somewhat inconsistent. Efforts have been made to mitigate the problem by taking the dispersion of the Fermi surface in the ground state, known as the extended RPA (ERPA) [31, 47]. The ERPA

adopts an iteration procedure. Starting from the HF ground state, the initial amplitudes $\boldsymbol{X}$ and $\boldsymbol{Y}$ are determined using Eqs. (7) and (9), and are used to calculate one-body densities of the correlated ground state [48]. After this step, new matrix elements in Eq. (8) which depend on the density are calculated, and then new amplitudes $\boldsymbol{X}$ and $\boldsymbol{Y}$ are obtained. The iterative procedure is repeated until convergence is reached. However, it turns out that the effect of the ground-state correlation on collective multipole resonances is rather small [31]. As commented in Ref. [46], the calculations of the double commutators should be less sensitive to the choice of the ground state $|0\rangle$. In this paper we will not use this approach, but we will calculate a correction to the ground state energy as described below.

B. The ground-state correlation

The RPA calculates relative quantities, such as excitation energy and transition densities. It does not pay much attention to the ground state explicitly. Following the QB approximation, the total binding energy of the ground state can be evaluated by considering contributions from the zero-point energies of all possible particle-hole excitation modes [45],

$$\mathrm{E_{RPA\text{-}QB}} = E_{\mathrm{HF}} - \frac{1}{2}\mathrm{Tr}\ \mathbf{A} + \frac{1}{2}\sum_{\nu}\hbar\Omega_{\nu}, \tag{12}$$

where Tr $\mathbf{A}$ is the trace of all the $\mathbf{A}^J$ matrices appearing in Eq. (7)-(9), and the summation is over all possible particle-hole excitation modes including charge exchange excitations where isospins are changed. The particle-hole excitations can have various coupled spins and parities allowed in the truncated model space. For example, in the ^{16}O calculation, the coupled spins and parities are from $0^{\pm}$ to $14^{\pm}$ in the basis truncation with $N_{\max} = 12$.

It has been known that the QB approximation overestimates the correlation energy. In Ref. [49] it was shown that the coupled-cluster doubles equation including only ring terms (ring-CCD) is equivalent to RPA, except for a factor of 1/2 in the ring-CCD correlation energy. More precisely, by comparing the contributions from the ring diagrams of many body perturbation theory (MBPT) to all orders, the RPA correlation energy from the QB approximation is overestimated by a factor of two in the second-order perturbation diagram [50]. This means that the a better approximation to the ground-state energy can be obtained by subtracting the second-order correlation term,

$$\mathrm{E_{RPA}} = \mathrm{E_{RPA\text{-}QB}} - \mathrm{E}^{(2)}, \tag{13}$$

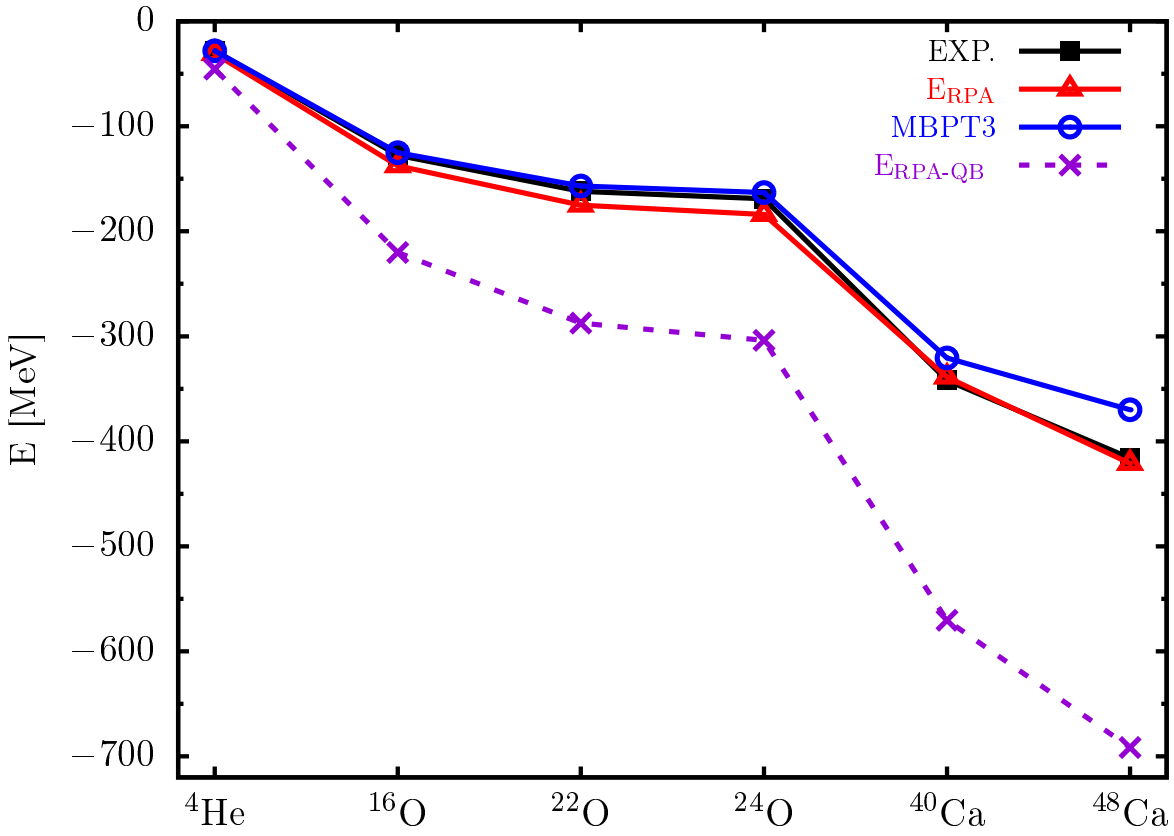

FIG. 1. Calculated RPA ground-state energy with the second-order MBPT correction (E_{RPA}), compared with MBPT3 calculations and experimental data. The quasi-boson RPA energy ($E_{RPA\text{-}QB}$) given by Eq. (12) is also displayed for comparison. The chiral $NNLO_{sat}$ interaction is used. We take $\hbar\omega = 22$ MeV for the harmonic oscillator basis and truncate the basis with $N_{max} = 2n + l = 12$.

where $E^{(2)}$ is the second-order perturbation diagram [51]. The binding energy calculation now includes contributions from all ring diagrams. In energy calculations based on realistic nuclear forces, this second-order correction plays an important role [51]. Fig. 1 shows the uncorrected ($E_{RPA\text{-}QB}$) and corrected (E_{RPA}) binding energies, and MBPT calculations up to third-order (MBPT3), compared with experimental data. The chiral interaction, $NNLO_{sat}$ [37], was used for these calculations, where the three-body force was truncated at the normal-ordered two-body level in the Hartree-Fock basis. We see that the usual RPA energy given by Eq. (12) without the $E^{(2)}$ correction gives poor results, and that the $E^{(2)}$ correction plays a crucial role.

C. Responses and transitions

The nuclear response to the electromagnetic field can be described by multipole operators ($O_{\lambda\mu}$) that come from a multipole expansion of the nuclear coupling with the field [52]. In the long-wavelength limit, the lowest-order electric multipole transition operators of interest are given below.

The isoscalar monopole operator is defined as

$$O_{00}^{\rm IS} = \sum_{i=1}^{A} r_i^2, \tag{14}$$

where $r_i = |\boldsymbol{r}_i|$ is the distance in radius for the i-th nucleon. The effective isovector dipole operator with the center-of-mass motion removed is

$$\begin{aligned} O_{1\mu}^{\rm IV} &= e\frac{N}{A}\sum_{i=1}^{Z} r_i Y_{1\mu}(\hat{\boldsymbol{r}}_i) - e\frac{Z}{A}\sum_{i=1}^{N} r_i Y_{1\mu}(\hat{\boldsymbol{r}}_i) \\ &= e\sum_{i=1}^{A}(\frac{N-Z}{2A} - t_z^{(i)}) r_i Y_{1\mu}(\hat{\boldsymbol{r}}_i), \end{aligned} \tag{15}$$

where N and Z are the neutron and proton numbers, respectively, e is the charge of a proton, $Y_{\lambda\mu}(\hat{\boldsymbol{r}}_i)$ is the spherical harmonics for the multipole mode ($\lambda\mu$), while $t_z^{(i)}$ is the isospin projection of the i-th nucleon. The isoscalar dipole operator [53] that corresponds to the compressional dipole mode is

$$O_{1\mu}^{\rm IS} = \sum_{i=1}^{A} r_i^3 Y_{1\mu}(\hat{\boldsymbol{r}}_i). \tag{16}$$

For the multipolarity $l \geq 2$ isoscalar operators, the usual forms are taken as

$$O_{l\mu}^{\rm IS} = \sum_{i=1}^{A} r_i^l Y_{l\mu}(\hat{\boldsymbol{r}}_i). \tag{17}$$

We have omitted the charge e in isoscalar operators, since the transition is not necessarily induced by the electromagnetic interaction. In the $J^\pi = 1^-$ dipole channel, a spurious state associated with the center-of-mass motion emerges as the HF breaks the transitional symmetry. In principle, the energy of the spurious state is exactly zero in the RPA [45], which gives an easy way to identify the spurious state. In practice, the energy of the spurious state is not exactly zero due to a limited model space. It is, however, close to zero and well separated from other states. For example, in our calculations with a model space of

$N_{\max} = 12$ the energies of the spurious states in ^{4}He and ^{16}O are as small as 10^{-15} MeV. The maximum energy of the spurious state happens in ^{48}Ca, where it is 0.8 MeV, well separated from the lowest resonance peak at ≈ 11 MeV. Therefore, we can easily identify and remove the 1^- spurious state.

The reduced l-pole electric transition probability is given by

$$\begin{aligned} B(El, 0 \to \nu) &= \sum_{\mu} |\langle \nu | O_{l\mu} | 0 \rangle|^2 \\ &\approx |\sum_{ph} (X^{l*}_{ph} + (-1)^l Y^{l*}_{ph}) \langle p \| o_l \| h \rangle|^2, \end{aligned} \tag{18}$$

where $\langle p \| o_l \| h \rangle$ is the reduced matrix element of the single transition operator, e.g., $o_l = r^3 Y_{1\mu}(\hat{\boldsymbol{r}})$ for an isoscalar dipole mode. Because we are discussing the transition between the 0^+ ground state and excited state ν with an angular momentum J, we have $l = J$.

The response strength distribution against excitation energy E is given by

$$R(E) = \sum_{\nu} B(EJ) \delta(E - \hbar\Omega_\nu). \tag{19}$$

The above discrete distribution is smoothed using the Lorentzian function to simulate escaping and spreading widths. Finally, we obtain the continuous strength function,

$$R(E) = \sum_{\nu} B(EJ) \frac{1}{\pi} \frac{\Gamma/2}{(E - \hbar\Omega_\nu)^2 + (\Gamma/2)^2}, \tag{20}$$

where the width of $\Gamma = 2$ MeV is used in this paper. This is a typical value for Γ that has been adopted in the literature (see e.g. Ref. [30, 31]).

The transition density can give detailed information about the resonance, which is defined as the transition amplitude of the density operator. For the state $|\nu\rangle$, the radial transition density is defined as

$$\begin{aligned} \delta\rho^J_\nu(r) &= \sum_{\mu} \langle \nu | \sum_i \frac{\delta(r - r_i)}{r^2} Y_{J\mu}(\hat{\boldsymbol{r}}_i) | 0 \rangle \\ &\approx \sum_{ph} (X^{J*}_{ph} + (-1)^J Y^{J*}_{ph}) \langle p \| \frac{\delta(r - r_i)}{r^2} Y_{J\mu}(\hat{\boldsymbol{r}}_i) \| h \rangle, \end{aligned} \tag{21}$$

where for the proton (neutron) transition density, the summation runs over the protons (neutrons) only.

III. CALCULATIONS AND DISCUSSIONS

In the present paper, we use the chiral $\mathrm{NNLO_{sat}}$ potential to calculate collective multipole resonances within the framework of the random phase approximation. We focus on monopole, dipole and quadrupole resonances which have been observed in various experiments. The $\mathrm{NNLO_{sat}}$ interaction contains the NNN force in the normal-ordered two-body approximation [40, 41]. The NNN effects on the giant resonances of light nuclei have been investigated with few-body *ab-initio* approaches [24, 25, 28, 29]. In Refs. [24, 25], with the Argonne NN and Urbana NNN forces, the authors used the correlated hyperspherical harmonics method to calculate the photodisintegrations of the giant dipole resonances in ^{3}H, ^{3}He and ^{4}He. The chiral potential with N^{3}LO (NN) and N^{2}LO (NNN) was used for the ^{4}He giant monopole resonance within the *ab-initio* few-body Jacobi coordinates [29] and for the ^{4}He giant dipole resonance with no core shell model [28]. The calculations indicate that the NNN effects appear mainly for high excitation energies ($E_x > 50$ MeV), increasing total resonance cross sections.

Fig. 2 shows the $\mathrm{NNLO_{sat}}$-RPA calculations of strength distributions for isoscalar giant monopole resonances (ISGMR), isovector giant dipole resonances (IVGDR) and isoscalar giant quadrupole resonances (ISGQR) in ^{40}Ca. For comparison, we have also shown results using the chiral N^{3}LO (NN) potential from Entem and Machleidt [42], softened to various cutoffs using the $V_{\mathrm{low}\text{-}k}$ method [44]. We first performed a spherical HF calculation in a harmonic oscillator basis, then used the normal-ordered two-body approximation [40, 41] to arrive at a two-body interaction used in the residual RPA *ph* calculations. We see that the $\mathrm{NNLO_{sat}}$ calculations are in overall agreement with experimental resonance peaks, while the N^{3}LO (NN) calculations are sensitive to the $V_{\mathrm{low}\text{-}k}$ momentum cutoff parameter Λ. No single Λ value is found to describe ISGMR, IVGDR and ISGQR simultaneously. The dependence on the softening parameter has been commented in the RPA calculations based on the AV18 potential by the unitary correlation operator method (UCOM) [30]. This is a clear indication that induced three-body forces must be included for this approach to be valid. With the coupled-cluster method, the bare N^{3}LO (NN) interaction was successfully applied to ^{4}He, ^{16,22}O and ^{40}Ca giant dipole resonances [35, 36]. Using bare forces, there are no induced three-body forces, however explicit three-body forces must still be considered.

According to the macroscopic interpretation of the giant dipole resonance by the Goldhaber-

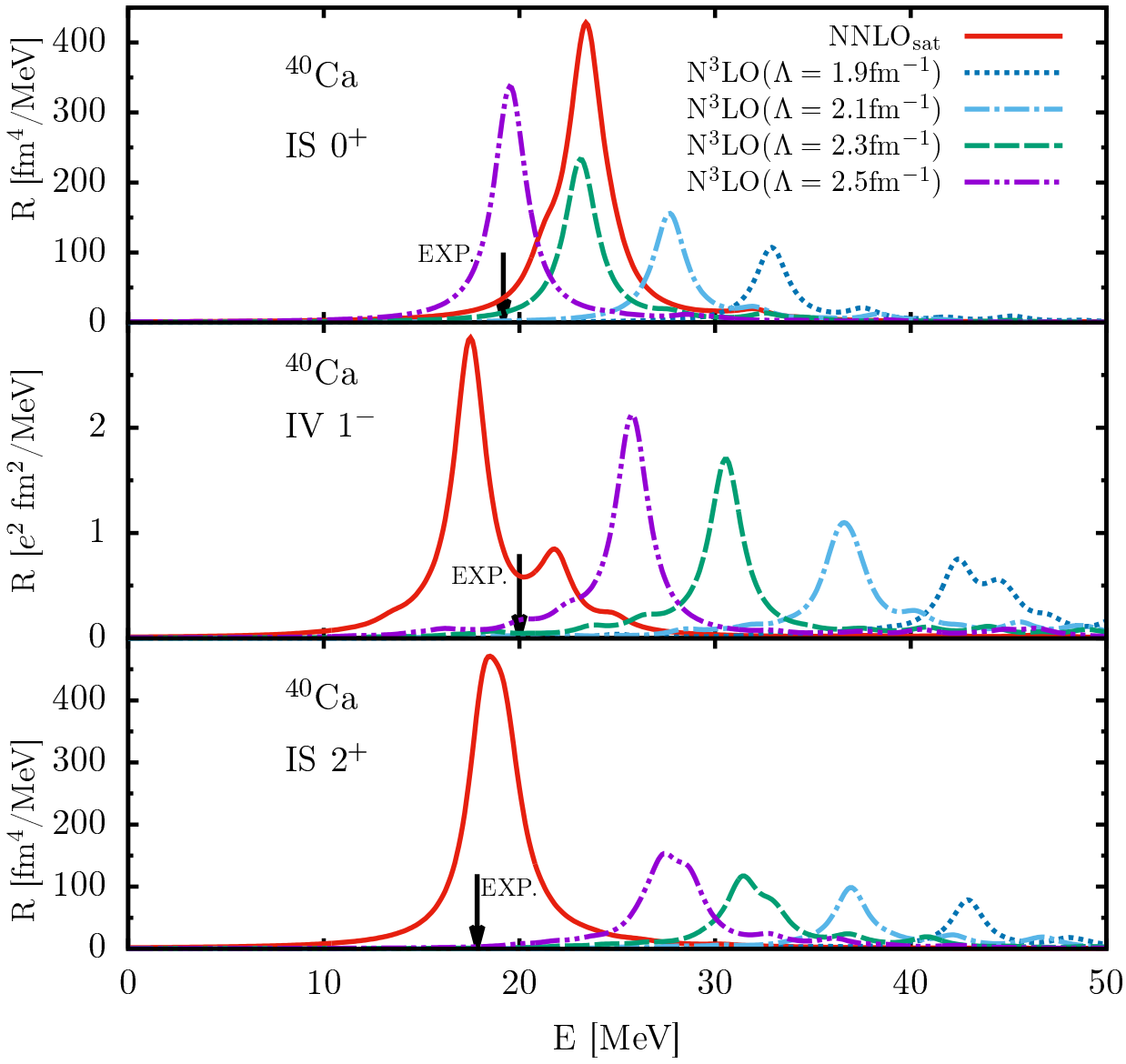

FIG. 2. Calculated ^{40}Ca isoscalar (IS) and isovector (IV) strength distributions using NNLO$_{sat}$ and N^{3}LO (at different V$_{low\text{-}k}$ cutoff Λ). The experimental centroid energies from [3, 54] are indicated by arrows. The harmonic oscillator basis parameter $\hbar\omega$ and the basis truncation N_{max} are same as in Fig. 1.

Teller [55] or Steinwedel-Jensen model [56], the resonance energy is inversely proportional to the radius of the nucleus. It has been known that *ab-initio* calculations based on realistic two-body interactions neglecting three-body forces give smaller radii compared with experimental data [37, 51, 57, 58]. NNLO$_{sat}$ is optimized with nuclear radii [37], which improves

the descriptions of nuclear bulk properties including nuclear electric dipole polarizabilities [38, 39]. Table I shows the calculated charge radii using $\mathrm{NNLO_{sat}}$, compared with the experimental data. The calculated charge radius r_{ch} is obtained from the HF point-proton radius r_{pp} using the standard expression [37]: $\langle r^2_{\mathrm{ch}}\rangle = \langle r^2_{\mathrm{pp}}\rangle + R^2_{\mathrm{p}} + \frac{N}{Z}R^2_{\mathrm{n}} + \frac{3\hbar^2}{4m_p^2c^2}$, where $\frac{3\hbar^2}{4m_p^2c^2} = 0.033$ fm^2, $R^2_{\mathrm{n}} = -0.1149(27)$ fm^2, $R_{\mathrm{p}} = 0.8775(51)$ fm. For comparison, we also give the $\mathrm{NNLO_{sat}}$ calculations of the radii with the coupled-cluster method in the singles and doubles approximation (CCSD) [37]. We see that the calculated charge radii using $\mathrm{NNLO_{sat}}$ are in good agreement with the experimental data. It would be interesting to calculate nuclear matter using $\mathrm{NNLO_{sat}}$. Unfortunately, we have not been able to calculate the properties of nuclear matter using the present model. It is not as straightforward as in energy density functional theory. However, in Ref. [37], the coupled-cluster method with $\mathrm{NNLO_{sat}}$ has calculated some properties of symmetric nuclear matter, giving an incompressibility of K=253 MeV which agrees with the empirical value [59].

1. Monopole resonances

The ISGMR is a breathing mode in which neutrons and protons move in phase. The ISGMR excitation energy is connected to the incompressibility of nuclear matter [64]. It provides important information on nuclear matter which cannot be probed directly in ordinary laboratories.

The calculated ISGMR strength distributions using $\mathrm{NNLO_{sat}}$ are displayed in Fig. 3

TABLE I. $\mathrm{NNLO_{sat}}$(NN+NNN) calculated charge radii (in fm) with the HF and CCSD [37] approximations for ^{4}He, ^{16,22,24}O and ^{40,48}Ca, compared with available experimental data [60, 61].

	Present	CCSD	Expt.
^{4}He	1.76	-	1.6755(28)
^{16}O	2.76	2.71	2.6991(52)
^{22}O	2.75	2.72	-
^{24}O	2.78	2.76	-
^{40}Ca	3.47	3.48	3.4776(19)
^{48}Ca	3.46	-	-

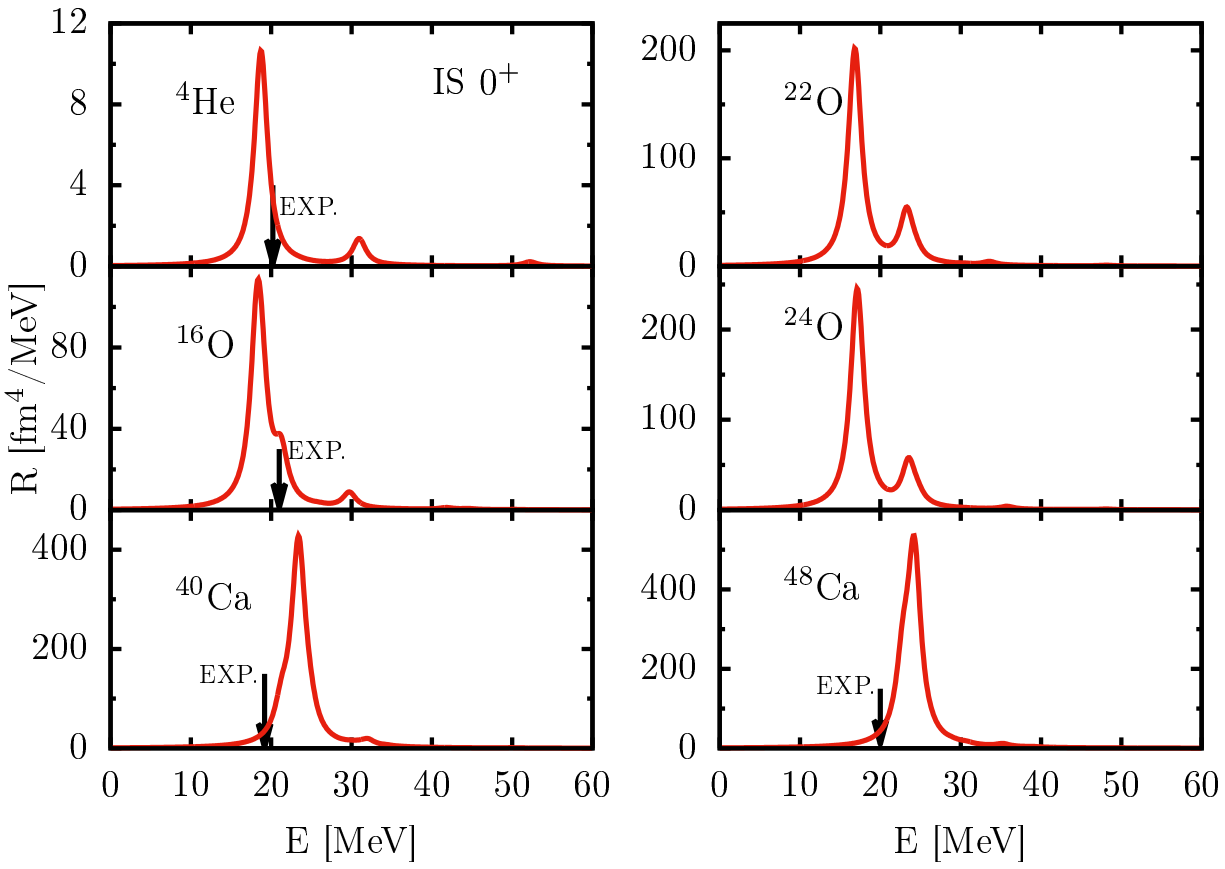

FIG. 3. Calculated strength distributions of isoscalar monopole resonance using $\mathrm{NNLO_{sat}}$. The experimental centroid energies are indicated by arrows. Experimental data are taken from Refs. [62] (^{16}O), [54] (^{40}Ca), [63] (^{48}Ca). For ^{4}He, the first excited state energy is adopted as the centroid energy [29]. The harmonic basis parameter and basis truncation are same as Fig. 1.

for the closed-shell nuclei, ^{4}He, ^{16,22,24}O and ^{40,48}Ca. The centroid energies obtained from experimental data with inelastic (α, α') scattering are given for comparison. For ^{4}He, our calculations show that the first 0^+ excited state has a breathing excitation mode, consistent with Ref. [29]. We see that the present calculations are in reasonable agreement with the available data. The small discrepancies ($\approx$ 1–4 MeV) between the calculations and data could originate from missing correlations in RPA.

2. Dipole resonances

The IVGDR has been the subject of a large number of studies. Many of these have focused on low-lying dipole strengths in nuclei away from the valley of stability [14, 65].

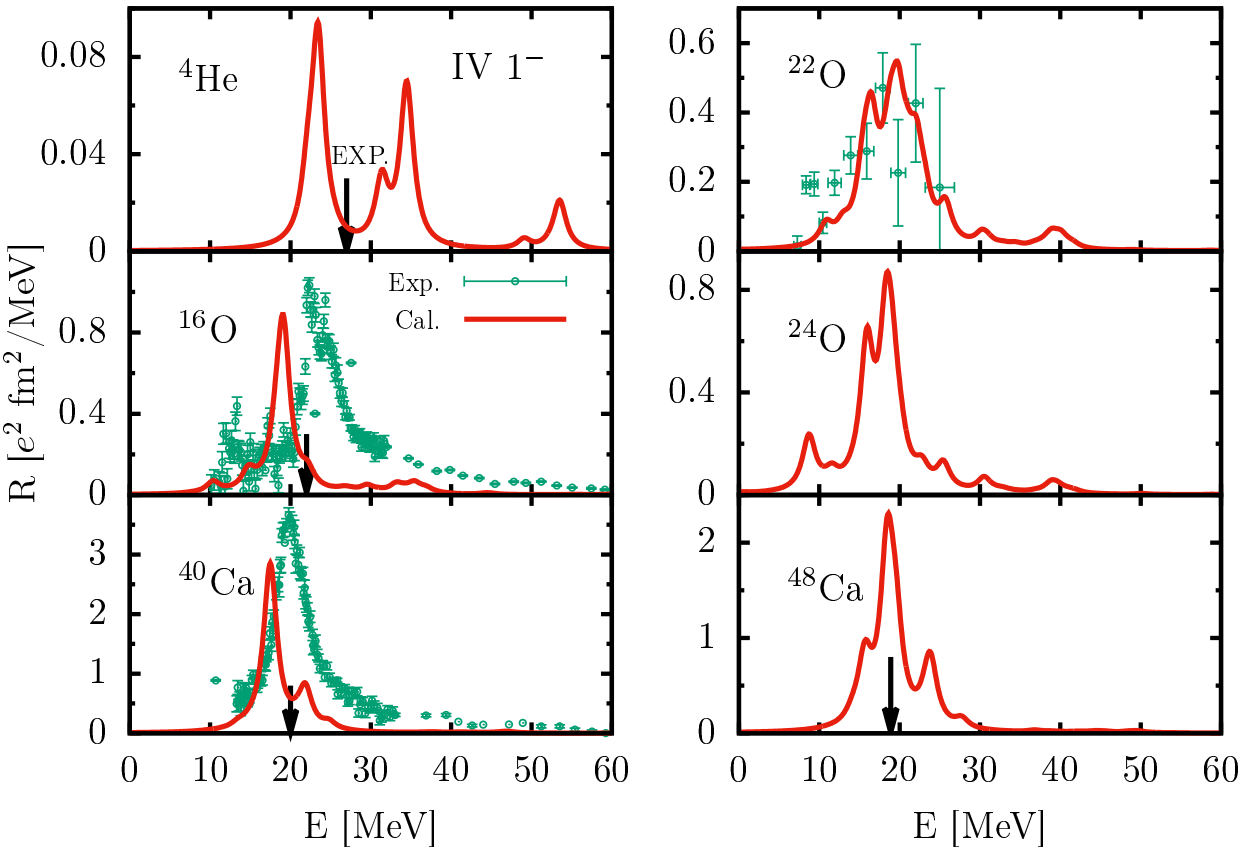

FIG. 4. Calculated strength distributions of isovector dipole resonances using NNLO$_{sat}$. The experimental centroid energies are indicated by arrows. Experimental centroids are taken from [66] for ^{48}Ca, and [3] for other nuclei. The experimental photoabsorption cross sections for ^{16}O, ^{22}O and ^{40}Ca are from Refs. [67–69]. The harmonic oscillator basis parameter $\hbar\omega$ and the basis truncation $N_{\max}$ are same as in Fig. 1.

Isovector resonances are connected to the symmetry energy and the slope of the symmetry-energy curve, and thus provide critical information of constraints on the equation of state of nuclear matter [8].

In Fig. 4, the calculated isovector dipole strength distributions are displayed and compared to experimental data. The calculations are in reasonable agreement with experiments. For ^{16,22}O and ^{40}Ca, the strength functions extracted from experimental photoabsorption cross sections are also displayed. The centroid energies obtained from RPA calculations are about 1–3 MeV lower than the experimental data. This may be improved by including additional many-body correlations.

In literature, the enhancement factor for the Thomas-Reiche-Kuhn (TRK) sum rule is widely used to characterize the size of momentum-dependent and isospin exchange contributions in the employed nuclear force [21]. The TRK sum rule reads [70]

$$S(E1) = \sum_{\nu} \hbar\Omega_{\nu} B(E1, 0 \to \nu) = \frac{\hbar^2 e^2}{2m} \frac{9}{4\pi} \frac{NZ}{A} (1 + \kappa), \tag{22}$$

where κ is the so-called enhancement factor. Table II summarizes the TRK sum-rule enhancement factor obtained in our NNLO$_{\rm sat}$ calculations by intergrating the strength functions. The calculated values are consistent with other calculations with the chiral N^{3}LO interaction [36].

The plots for ^{22}O and ^{24}O show evidence of low-lying strengths around 10 MeV. It is more pronounced in ^{24}O. This low-energy resonance is usually called the pygmy dipole resonance (PDR), which is interpreted as the oscillation of excess neutrons against the $N = Z$ core. In our calculations, the strength below 15 MeV exhausts about 4.3% of the classical TRK sum rule in ^{22}O, while 10.7% in ^{24}O. The experimental data of ^{22}O give about 8% of the classical TRK sum rule up to excitation energy of 15 MeV [69].

To investigate the nature of these resonances, we calculate transition densities shown in Figs. 5 and 6 for ^{22}O and ^{24}O at the prominent peaks. For the ^{22}O peak at 10.8 MeV, the protons and neutrons oscillate in phase in the interior, while in the surface region the neutron transition density dominates. This is consistent with a PDR. At the higher resonance peaks, the transition densities show that the protons and neutrons oscillate out of phase, exhibiting the typical and well-known picture of a GDR. Fig. 6 shows a similar behavior in the transition densities of ^{24}O. The present results are consistent with the relativistic RPA calculations given in Refs. [71, 72]. It was discussed that low-energy soft dipole resonances in halo nuclei have similar in-phase transition densities [13, 73]. The soft dipole resonance appears due to the oscillation of the halo neutrons against a core. The excitation energy of the soft resonance is low, e.g., $\approx 2 - 3$ MeV in ^{6}He, ^{11}Li and ^{12}Be [13, 73]. The low-energy

TABLE II. The TRK sum-rule enhancement factor κ obtained in the present NNLO$_{\rm sat}$ calculations for ^{4}He, ^{16,22,24}O and ^{40,48}Ca.

	^{4}He	^{16}O	^{22}O	^{24}O	^{40}Ca	^{48}Ca
κ	0.57	0.53	0.56	0.55	0.56	0.58

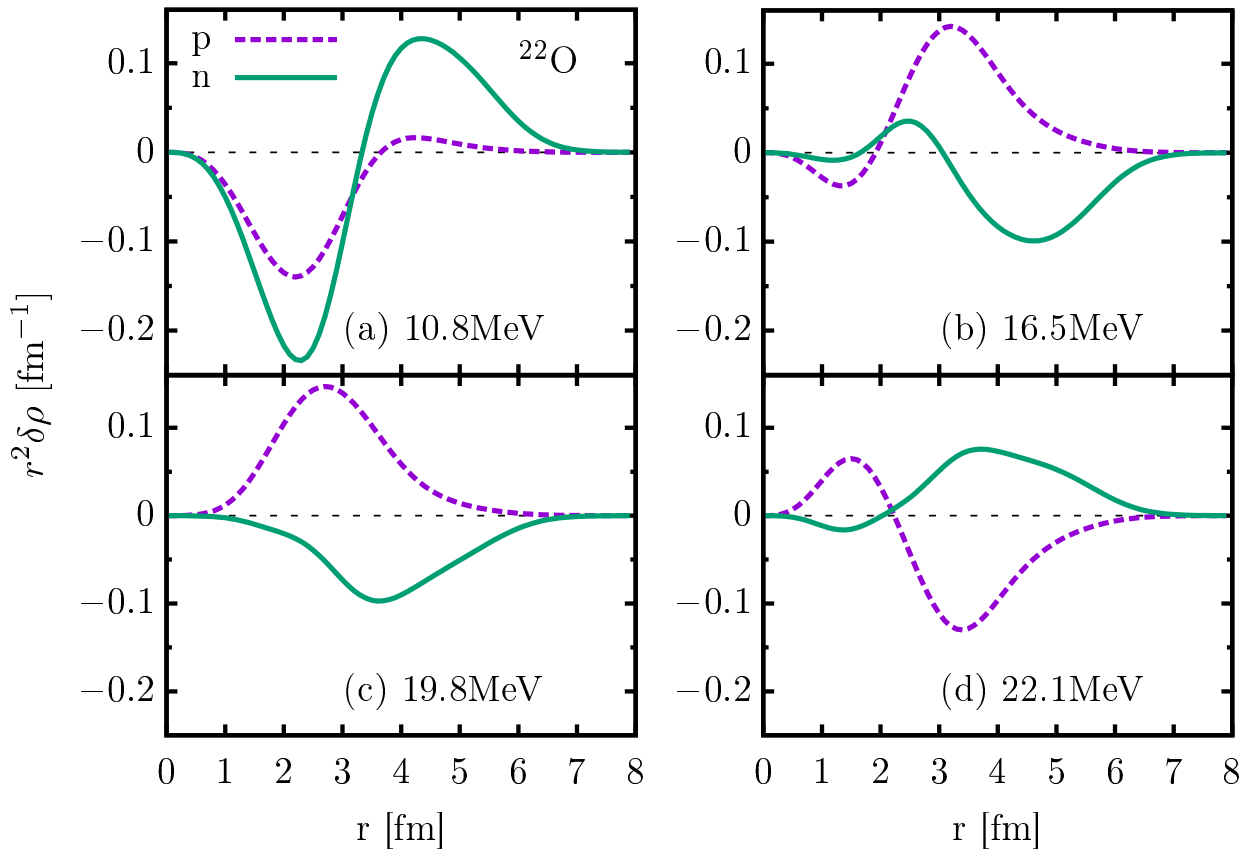

FIG. 5. Calculated ^{22}O transition densities for the protons and neutrons at the prominent peaks of the dipole resonance: (a) 10.8 MeV, (b) 16.5 MeV, (c) 19.8 MeV and (d) 22.1 MeV.

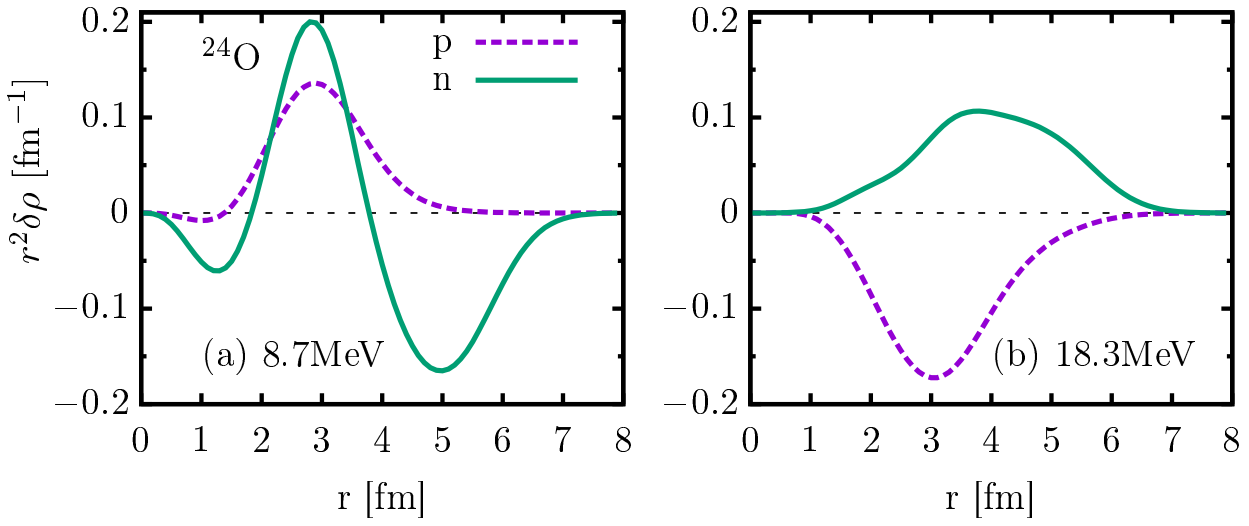

FIG. 6. Calculated ^{24}O transition densities for the protons and neutrons at the prominent peaks of the dipole resonance: (a) 8.7 MeV and (b) 18.3 MeV.

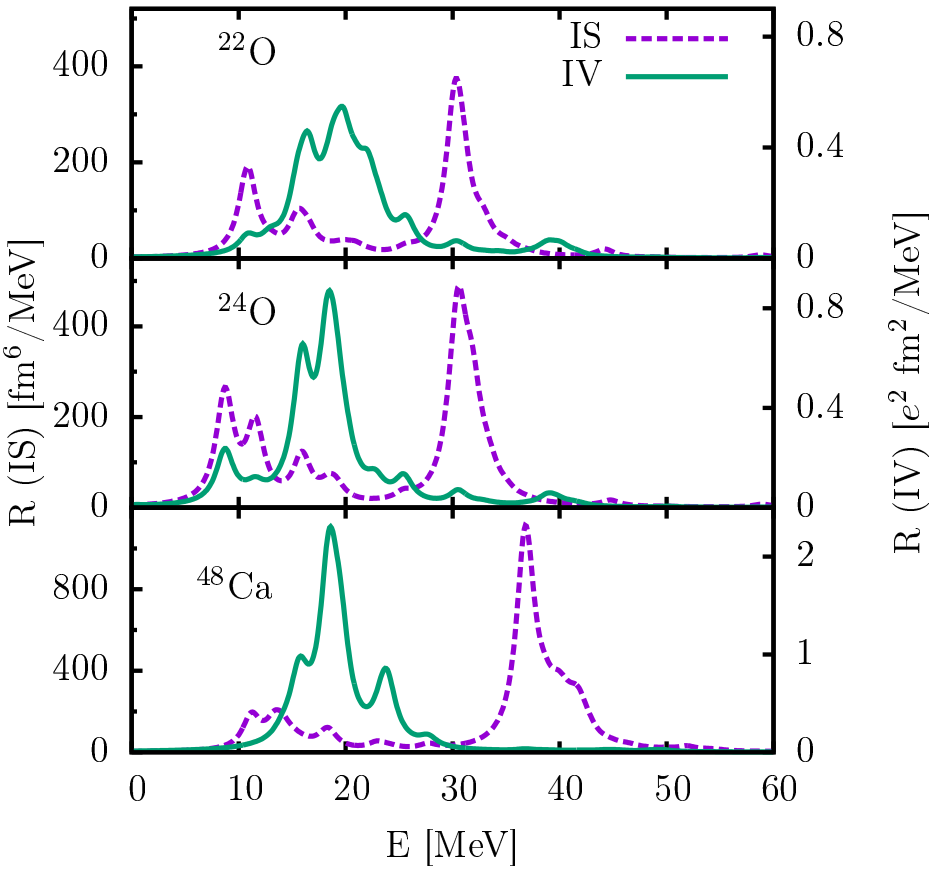

FIG. 7. Comparison of isoscalar and isovector dipole resonance strength distributions. For visibility, different scales have been used for the isoscalar (left) and isovector (right) channels.

dipole strength in light neutron-rich nuclei is interpreted as mainly arising from single-neutron transitions rather than showing much collectivity [65, 74]. The oxygen isotopes ^{22,24}O have larger neutron separation energies than the loosely bound light nuclei, thus the low-energy strengths are less pronounced because of the threshold effect [75].

The RPA formalism also provides a way to analyze the wave function of a peak state. For ^{22}O, the main components of the wave function for the excited state at 10.8 MeV are the neutron excitations: 62% $0d_{5/2} \rightarrow 1p_{3/2}$, 15% $0p_{1/2} \rightarrow 1s_{1/2}$ and 8% $0d_{5/2} \rightarrow 0f_{7/2}$, while relativistic RPA calculations give 93% $0d_{5/2} \rightarrow 1p_{3/2}$ and 3% $0d_{5/2} \rightarrow 0f_{7/2}$ [71]. For ^{24}O, the main components for the state at 8.7 MeV are the neutron excitations: 87% $1s_{1/2} \rightarrow 1p_{3/2}$ and 5% $0d_{5/2} \rightarrow 0f_{7/2}$, while relativistic RPA calculations give 93% for the neutron particle-hole excitation $1s_{1/2} \rightarrow 1p_{3/2}$.

The PDR mode is of special interest in neutron-rich nuclei [76]. The transition densities

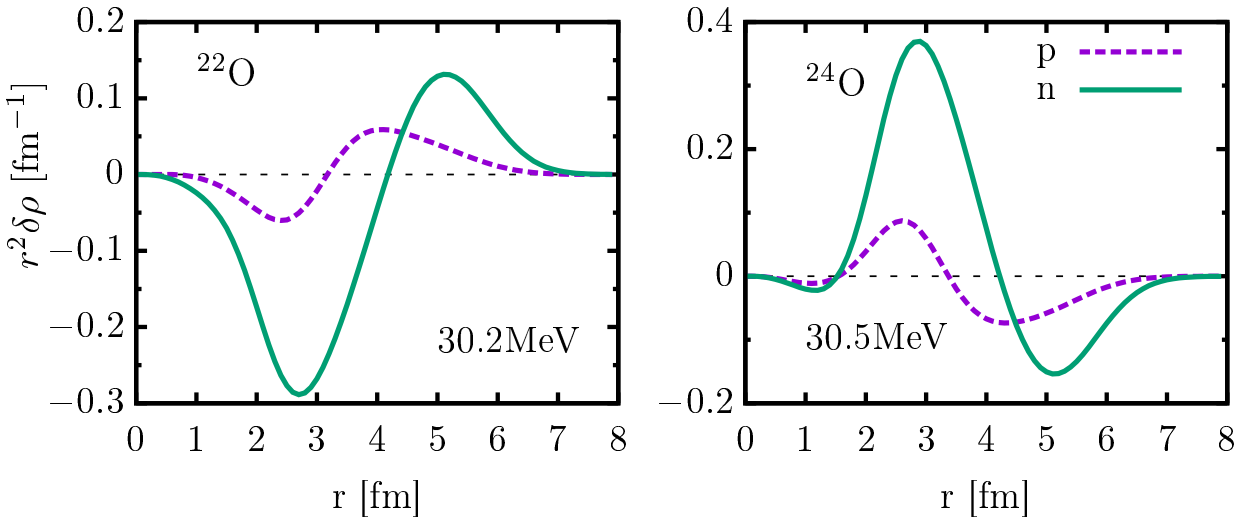

FIG. 8. Calculated ^{22}O and ^{24}O transition densities for the protons and neutrons at the main peaks of the isoscalar dipole resonances around 30 MeV.

indicate that the low-lying strengths are mainly of isoscalar nature, see the subfigures (a) in Figs. 5 and 6. However, Fig. 7 contrasts the isoscalar dipole resonance (isoscalar compressional dipole mode) strength distributions with the isovector dipole resonances for ^{22}O, ^{24}O and ^{48}Ca, and shows that for ^{22}O and ^{24}O, the low-energy peaks of the isoscalar and isovector channels appear at the same energy. This indicates that the PDR excitation has a nature of isoscalar and isovector mixing. Fig. 8 shows the transition densities at the main peaks of the isoscalar dipole resonances around 30 MeV in Fig. 7 for ^{22,24}O. The strength distributions for ^{48}Ca does not display the similar mixing, as only an isoscalar peak is found at low-energy around 11 MeV. In experiment, low-energy ISGDR strengths can be obtained by the isoscalar compressional dipole transitions caused by inelastic scatterings with an isoscalar particle (e.g., α particle) [59], while excitations due to electromagnetic interaction (usually by electron scatterings) give the total strength of the ISGDR and IVGDR transitions. Therefore, the comparison of the scattering data may give the information about the isoscalar and isovector mixing.

3. Quadrupole resonances

Fig. 9 shows the calculated isoscalar quadrupole strength distributions, as well as the available experimental centroid energies. The calculations are in good agreement with ex-

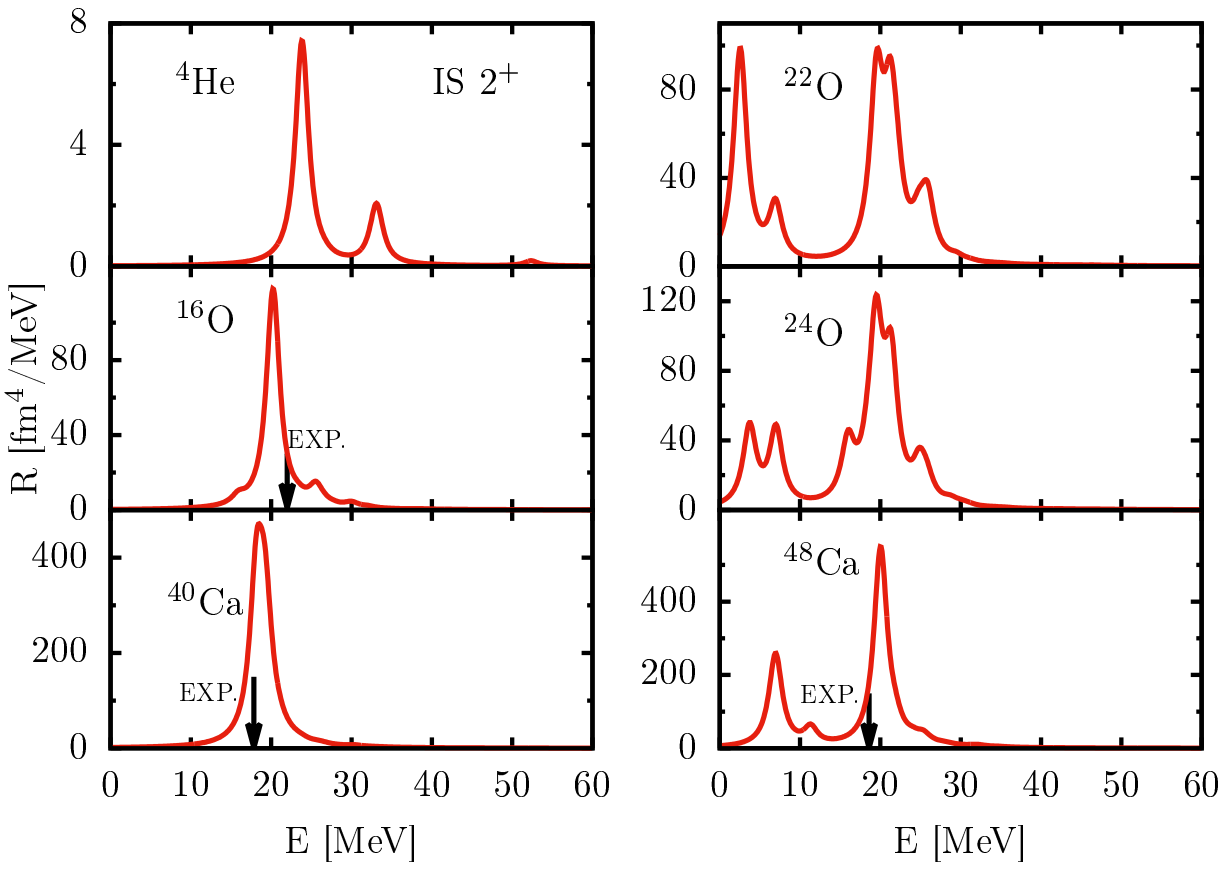

FIG. 9. Calculated strength distributions of isoscalar quadrupole resonance using NNLO$_{\rm sat}$. The experimental centroid energies are indicated by arrows. Experimental data are taken from Refs. [62] (^{16}O), [54] (^{40}Ca), [63] (^{48}Ca). The harmonic basis parameter and basis truncation are same as in Fig. 1.

perimental data where available. It is interesting that the neutron-rich ^{22,24}O and ^{48}Ca have pronounced low-energy peaks in the calculated quadrupole strengths. The low-lying peak should be compared with the experimental excitation energy of the corresponding 2^+ state. We have analyzed the RPA wave function, and find that the low-lying peak is predominantly a single-neutron excitation. The calculated peak at 2.5 MeV in ^{22}O is a one-neutron excitation from $0d_{5/2}$ to $1s_{1/2}$, compared with the excitation energy of the observed first 2^+ state at 3.2 MeV [77]. For ^{24}O, the present calculations give that the low-energy peaks at 3.7 and 7.0 MeV are due to the single-neutron excitations from $1s_{1/2}$ to $0d_{3/2}$ and from $0d_{5/2}$ to $0d_{3/2}$, respectively, while the experimental 2^+_1 state energy is 4.7 MeV [78].

The present NNLO$_{\rm sat}$-RPA calculated excitation energies of the low-lying 2^+ resonance

states are also consistent with our previous calculations using the Gamow shell model (GSM) with the CD-Bonn potential [79] . The Gamow shell model takes into account resonance and continuum by using a complex-momentum Berggren coordinates. The GSM calculations give that ^{22}O has a 2^+ excited state at 3.3 MeV with a one-neutron excitation from $0d_{5/2}$ to $1s_{1/2}$ as the dominant configuration. The nucleus ^{24}O has a 2^+ resonance state at 4.5 MeV, dominated by a one-neutron excitation from $1s_{1/2}$ to $0d_{3/2}$ [79] . The energy gap between neutron $1s_{1/2}$ and $0d_{3/2}$ is larger than the gap between neutron $0d_{5/2}$ and $1s_{1/2}$.

IV. SUMMARY

In the present work, the chiral NNLO$_{\rm sat}$ potential, which includes a three-body force, has been used to investigate the monopole, dipole, and quadrupole resonances of the closed-shell nuclei ^{4}He, ^{16,22,24}O and ^{40,48}Ca. The calculations were done in the HF-RPA approach. Due to strong short-range correlations, the HF calculation based on realistic nuclear forces cannot give right binding energies of nuclei. The energy of the ground state is calculated by the RPA energy and a correction from second-order perturbation theory. The RPA NNLO$_{\rm sat}$ calculations reproduce the available experimental centroid energies of isoscalar monopole, isovector dipole and isoscalar quadrupole resonances of these nuclei reasonably well. The HF-RPA resonance calculations using a softened two-body realistic interaction without three-body force are sensitive to the softening parameter, indicating the importance of induced three-body force.

In neutron-rich ^{22}O and ^{24}O, we obtain low-energy dipole resonances at excitation energies around 10 MeV. The calculations of response strengths show that the low-energy resonances are a mix between isoscalar and isovector dipole resonances. However, the transition density calculations indicate that the low-energy dipole resonances are dominated by the isoscalar mode, while the dipole resonances at higher energies exhibit the characteristic of the isovector mode. The RPA calculations reveal that the low-energy dipole resonance is dominated by a single-neutron excitation, which is consistent with other RPA calculations based on phenomenological interactions. Prominent peaks at low energies between 2 and 7 MeV are found in the isoscalar quadrupole response functions of neutron-rich ^{22,24}O and ^{48}Ca. The low-energy quadrupole resonances are identified as single-neutron transitions. The peak positions are in reasonable agreement with the experimental energies of the corresponding

2^+ states and Gamow shell model calculations. The RPA calculation may be improved by including high-order correlations (e.g. $2p2h$, $3p3h\cdots$ excitations).

ACKNOWLEDGMENTS

Valuable discussions with T. Papenbrock, U. Garg, J. P. Vary and J.C. Pei are gratefully acknowledged. This work has been supported by the National Natural Science Foundation of China under Grants No. 11235001, No. 11320101004 and No. 11575007; and the CUSTIPEN (China-U.S. Theory Institute for Physics with Exotic Nuclei) funded by the U.S. Department of Energy, Office of Science under Grant No. DE-SC0009971. This work was partially supported by the Office of Nuclear Physics, U.S. Department of Energy, under Grants DE-FG02-96ER40963, DE-SC0008499 (NUCLEI SciDAC collaboration), the Field Work Proposal ERKBP57 at Oak Ridge National Laboratory (ORNL), and used resources of the Oak Ridge Leadership Computing Facility located at ORNL, which is supported by the Office of Science of the Department of Energy under Contract No. DE-AC05-00OR22725. Computer time was partially provided by the Innovative and Novel Computational Impact on Theory and Experiment (INCITE) program.

[1] W. Bothe and W. Gentner, Z. Phys. **106**, 236 (1937).

[2] G. C. Baldwin and G. S. Klaiber, Phys. Rev. **71**, 3 (1947).

[3] B. L. Berman and S. C. Fultz, Rev. Mod. Phys. **47**, 713 (1975).

[4] A. Migdal, J. Phys. Acad. Sci. USSR **8**, 331 (1944).

[5] U. Garg, Acta. Phys. Pol. B **42**, 659 (2011).

[6] D. Patel, U. Garg, M. Fujiwara, H. Akimune, G. Berg, M. Harakeh, M. Itoh, T. Kawabata, K. Kawase, B. Nayak, T. Ohta, H. Ouchi, J. Piekarewicz, M. Uchida, H. Yoshida, and M. Yosoi, Physics Letters B **718**, 447 (2012).

[7] Y. Gupta, U. Garg, K. Howard, J. Matta, M. enyiit, M. Itoh, S. Ando, T. Aoki, A. Uchiyama, S. Adachi, M. Fujiwara, C. Iwamoto, A. Tamii, H. Akimune, C. Kadono, Y. Matsuda, T. Nakahara, T. Furuno, T. Kawabata, M. Tsumura, M. Harakeh, and N. Kalantar-Nayestanaki, Physics Letters B **760**, 482 (2016).

[8] G. Colò, U. Garg, and H. Sagawa, Eur. Phys. J. A **50**, 26 (2014).

[9] J. S. Brzosko, E. Gierlik, A. S. Jr., and Z. Wilhelmi, Canadian Journal of Physics **47**, 2849 (1969).

[10] R. Mohan, M. Danos, and L. C. Biedenharn, Phys. Rev. C **3**, 1740 (1971).

[11] P. G. Hansen and B. Jonson, EPL (Europhysics Letters) **4**, 409 (1987).

[12] Y. Suzuki, K. Ikeda, and H. Sato, Progress of Theoretical Physics **83**, 180 (1990).

[13] D. Mikami, W. Horiuchi, and Y. Suzuki, Phys. Rev. C **89**, 064303 (2014).

[14] N. Paar, D. Vretenar, E. Khan, and G. Colò, Reports on Progress in Physics **70**, 691 (2007).

[15] D. Savran, T. Aumann, and A. Zilges, Progress in Particle and Nuclear Physics **70**, 210 (2013).

[16] R. Kanungo, A. Sanetullaev, J. Tanaka, S. Ishimoto, G. Hagen, T. Myo, T. Suzuki, C. Andreoiu, P. Bender, A. A. Chen, B. Davids, J. Fallis, J. P. Fortin, N. Galinski, A. T. Gallant, P. E. Garrett, G. Hackman, B. Hadinia, G. Jansen, M. Keefe, R. Krücken, J. Lighthall, E. McNeice, D. Miller, T. Otsuka, J. Purcell, J. S. Randhawa, T. Roger, A. Rojas, H. Savajols, A. Shotter, I. Tanihata, I. J. Thompson, C. Unsworth, P. Voss, and Z. Wang, Phys. Rev. Lett. **114**, 192502 (2015).

[17] I. Tanihata, H. Savajols, and R. Kanungo, Progress in Particle and Nuclear Physics **68**, 215 (2013).

[18] M. Vandebrouck, J. Gibelin, E. Khan, N. L. Achouri, H. Baba, D. Beaumel, Y. Blumenfeld, M. Caamaño, L. Càceres, G. Colò, F. Delaunay, B. Fernandez-Dominguez, U. Garg, G. F. Grinyer, M. N. Harakeh, N. Kalantar-Nayestanaki, N. Keeley, W. Mittig, J. Pancin, R. Raabe, T. Roger, P. Roussel-Chomaz, H. Savajols, O. Sorlin, C. Stodel, D. Suzuki, and J. C. Thomas, Phys. Rev. Lett. **113**, 032504 (2014).

[19] L. Pellegri, A. Bracco, N. Tsoneva, R. Avigo, G. Benzoni, N. Blasi, S. Bottoni, F. Camera, S. Ceruti, F. C. L. Crespi, A. Giaz, S. Leoni, H. Lenske, B. Million, A. I. Morales, R. Nicolini, O. Wieland, D. Bazzacco, P. Bednarczyk, B. Birkenbach, M. Ciemała, G. de Angelis, E. Farnea, A. Gadea, A. Görgen, A. Gottardo, J. Grebosz, R. Isocrate, M. Kmiecik, M. Krzysiek, S. Lunardi, A. Maj, K. Mazurek, D. Mengoni, C. Michelagnoli, D. R. Napoli, F. Recchia, B. Siebeck, S. Siem, C. Ur, and J. J. Valiente-Dobón, Phys. Rev. C **92**, 014330 (2015).

[20] M. Spieker, N. Tsoneva, V. Derya, J. Endres, D. Savran, M. Harakeh, S. Harissopulos, R.-D. Herzberg, A. Lagoyannis, H. Lenske, N. Pietralla, L. Popescu, M. Scheck, F. Schlter, K. Sonnabend, V. Stoica, H. Wrtche, and A. Zilges, Physics Letters B **752**, 102 (2016).

[21] J. Erler, P. Klüpfel, and P.-G. Reinhard, Journal of Physics G: Nuclear and Particle Physics **38**, 033101 (201

[22] T. Nakatsukasa, Progress of Theoretical and Experimental Physics **2012**, 01A207 (2012).

[23] C. L. Bai, H. Q. Zhang, H. Sagawa, X. Z. Zhang, G. Colò, and F. R. Xu, Phys. Rev. Lett. **105**, 072501 (2010).

[24] V. D. Efros, W. Leidemann, G. Orlandini, and E. L. Tomusiak, Physics Letters B **484**, 223 (2000).

[25] D. Gazit, S. Bacca, N. Barnea, W. Leidemann, and G. Orlandini, Phys. Rev. Lett. **96**, 112301 (2006).

[26] R. B. Wiringa, V. G. J. Stoks, and R. Schiavilla, Phys. Rev. C **51**, 38 (1995).

[27] B. S. Pudliner, V. R. Pandharipande, J. Carlson, S. C. Pieper, and R. B. Wiringa, Phys. Rev. C **56**, 1720 (1997).

[28] S. Quaglioni and P. Navrátil, Physics Letters B **652**, 370 (2007).

[29] S. Bacca, N. Barnea, W. Leidemann, and G. Orlandini, Phys. Rev. C **91**, 024303 (2015).

[30] N. Paar, P. Papakonstantinou, H. Hergert, and R. Roth, Phys. Rev. **C74**, 014318 (2006).

[31] P. Papakonstantinou, R. Roth, and N. Paar, Phys. Rev. **C75**, 014310 (2007).

[32] P. Papakonstantinou and R. Roth, Phys. Rev. **C81**, 024317 (2010).

[33] H. Hergert, P. Papakonstantinou, and R. Roth, Phys. Rev. C **83**, 064317 (2011).

[34] R. Roth, T. Neff, H. Hergert, and H. Feldmeier, Nuclear Physics A **745**, 3 (2004).

[35] S. Bacca, N. Barnea, G. Hagen, G. Orlandini, and T. Papenbrock, Phys. Rev. Lett. **111**, 122502 (2013).

[36] S. Bacca, N. Barnea, G. Hagen, M. Miorelli, G. Orlandini, and T. Papenbrock, Phys. Rev. C **90**, 064619 (2014).

[37] A. Ekström, G. R. Jansen, K. A. Wendt, G. Hagen, T. Papenbrock, B. D. Carlsson, C. Forssén, M. Hjorth-Jensen, P. Navrátil, and W. Nazarewicz, Phys. Rev. C **91**, 051301 (2015).

[38] G. Hagen, A. Ekstrom, C. Forssen, G. R. Jansen, W. Nazarewicz, T. Papenbrock, K. A. Wendt, S. Bacca, N. Barnea, B. Carlsson, C. Drischler, K. Hebeler, M. Hjorth-Jensen, M. Miorelli, G. Orlandini, A. Schwenk, and J. Simonis, Nat Phys **12**, 186 (2016).

[39] M. Miorelli, S. Bacca, N. Barnea, G. Hagen, G. R. Jansen, G. Orlandini, and T. Papenbrock, Phys. Rev. C **94**, 034317 (2016).

[40] R. Roth, S. Binder, K. Vobig, A. Calci, J. Langhammer, and P. Navrátil, Phys. Rev. Lett. **109**, 052501 (2012).

[41] G. Hagen, T. Papenbrock, D. J. Dean, A. Schwenk, A. Nogga, M. Włoch, and P. Piecuch, Phys. Rev. C **76**, 034302 (2007).

[42] D. R. Entem and R. Machleidt, Phys. Rev. **C68**, 041001 (2003).

[43] R. Machleidt and D. R. Entem, Phys. Rept. **503**, 1 (2011).

[44] S. K. Bogner, T. T. S. Kuo, and A. Schwenk, Phys. Rept. **386**, 1 (2003).

[45] P. S. Peter Ring, *The Nuclear Many-Body Problem* (Springer, 2004).

[46] D. J. Rowe, Rev. Mod. Phys. **40**, 153 (1968).

[47] D. Gambacurta and F. Catara, Phys. Rev. B **77**, 205434 (2008).

[48] D. J. Rowe, Phys. Rev. **175**, 1283 (1968).

[49] G. E. Scuseria, T. M. Henderson, and D. C. Sorensen, The Journal of Chemical Physics **129**, 231101 (2008).

[50] P. Ellis, Nuclear Physics A **155**, 625 (1970).

[51] B. S. Hu, F. R. Xu, Z. H. Sun, J. P. Vary, and T. Li, Phys. Rev. **C94**, 014303 (2016).

[52] J. A. M. Walter Greiner, *Nuclear Models* (Springer, 1996).

[53] N. V. Giai and H. Sagawa, Nuclear Physics A **371**, 1 (1981).

[54] D. H. Youngblood, Y.-W. Lui, and H. L. Clark, Phys. Rev. C **63**, 067301 (2001).

[55] M. Goldhaber and E. Teller, Phys. Rev. **74**, 1046 (1948).

[56] H. Steinwedel, J. H. D. Jensen, and P. Jensen, Phys. Rev. **79**, 1019 (1950).

[57] S. Binder, J. Langhammer, A. Calci, and R. Roth, Physics Letters B **736**, 119 (2014).

[58] R. Roth, P. Papakonstantinou, N. Paar, H. Hergert, T. Neff, and H. Feldmeier, Phys. Rev. C **73**, 044312 (2006).

[59] U. Garg and G. Colò, (2018), arXiv:1801.03672 [nucl-ex].

[60] I. Angeli and K. Marinova, Atomic Data and Nuclear Data Tables **99**, 69 (2013).

[61] P. J. Mohr, B. N. Taylor, and D. B. Newell, Rev. Mod. Phys. **84**, 1527 (2012).

[62] Y. W. Lui, H. L. Clark, and D. H. Youngblood, Phys. Rev. C **64**, 064308 (2001).

[63] Y. W. Lui, D. H. Youngblood, S. Shlomo, X. Chen, Y. Tokimoto, Krishichayan, M. Anders, and J. Button, Phys. Rev. C **83**, 044327 (2011).

[64] J. Treiner, H. Krivine, O. Bohigas, and J. Martorell, Nuclear Physics A **371**, 253 (1981).

[65] T. Aumann and T. Nakamura, Physica Scripta **2013**, 014012 (2013).

[66] J. Birkhan, M. Miorelli, S. Bacca, S. Bassauer, C. A. Bertulani, G. Hagen, H. Matsubara, P. von Neumann-Cosel, T. Papenbrock, N. Pietralla, V. Y. Ponomarev, A. Richter,

A. Schwenk, and A. Tamii, Phys. Rev. Lett. **118**, 252501 (2017).

[67] J. Ahrens, H. Borchert, K. Czock, H. Eppler, H. Gimm, H. Gundrum, M. Krning, P. Riehn, G. S. Ram, A. Zieger, and B. Ziegler, Nuclear Physics A **251**, 479 (1975).

[68] CDFE database, `http://cdfe.sinp.msu.ru/services/gdrsearch.html`.

[69] A. Leistenschneider, T. Aumann, K. Boretzky, D. Cortina, J. Cub, U. D. Pramanik, W. Dostal, T. W. Elze, H. Emling, H. Geissel, A. Grünschloß, M. Hellstr, R. Holzmann, S. Ilievski, N. Iwasa, M. Kaspar, A. Kleinböhl, J. V. Kratz, R. Kulessa, Y. Leifels, E. Lubkiewicz, G. Münzenberg, P. Reiter, M. Rejmund, C. Scheidenberger, C. Schlegel, H. Simon, J. Stroth, K. Sümmerer, E. Wajda, W. Walús, and S. Wan, Phys. Rev. Lett. **86**, 5442 (2001).

[70] G. Orlandini and M. Traini, Reports on Progress in Physics **54**, 257 (1991).

[71] D. Vretenar, N. Paar, P. Ring, and G. Lalazissis, Nuclear Physics A **692**, 496 (2001).

[72] N. Paar, P. Ring, T. Nikšić, and D. Vretenar, Phys. Rev. C **67**, 034312 (2003).

[73] H. Sagawa and C. A. Bertulani, Progress of Theoretical Physics Supplement **124**, 143 (1996).

[74] H. Sagawa, N. Van Giai, N. Takigawa, M. Ishihara, and K. Yazaki, Zeitschrift für Physik A Hadrons and Nuclei **351**, 385 (1995).

[75] F. Catara, C. Dasso, and A. Vitturi, Nuclear Physics A **602**, 181 (1996).

[76] K. Wang, M. Kortelainen, and J. C. Pei, Phys. Rev. C **96**, 031301 (2017).

[77] M. S. Basunia, Nuclear Data Sheets **127**, 69 (2015).

[78] C. Hoffman, T. Baumann, D. Bazin, J. Brown, G. Christian, D. Denby, P. DeYoung, J. Finck, N. Frank, J. Hinnefeld, S. Mosby, W. Peters, W. Rogers, A. Schiller, A. Spyrou, M. Scott, S. Tabor, M. Thoennessen, and P. Voss, Physics Letters B **672**, 17 (2009).

[79] Z. Sun, Q. Wu, Z. H. Zhao, B. S. Hu, S. J. Dai, and F. R. Xu, Physics Letters B **769**, 227 (2017).